Title: Biological modifications of the immune response to COVID-19 vaccine in patients treated with anti-CD20 agents and immune-checkpoint inhibitors.

Authors: Ravera Francesco[1], Dameri Martina[2], Lombardo Isabella[2], Stabile Mario[1], Fallani Neri[2], Scarsi Camilla[1], Cigolini Benedetta[1], Gentilcore Giusy[3], Domnich Alexander[2], Zullo Lodovica[1], Cella Eugenia[1], Francia Giulia[1], Montanari Eugenia[1], Orsi Andrea[2], Bellodi Andrea[2], Ferrando Fabio[1,2], Rinchai Darawan[3,4], Ballerini Filippo[1,2], Bruzzone Bianca[2], Chaussabel Damien[5], Grivel Jean-Charles[6], Genova Carlo[1,2], Lemoli Roberto[1], Bedognetti Davide[1,7], Ballestrero Alberto[1,2,*,#], Ferrando Lorenzo[2,*,#], Zoppoli Gabriele[1,2,*,#]

[1]Department of Internal Medicine and Medical Specialties, University of Genoa, Genova (Italia)

[2]IRCCS Ospedale Policlinico San Martino, Genova, Italia

[3]Translational Medicine Division, Research Branch, Sidra Medicine, Doha (Qatar)

[4]Department of Infectious diseases, St. Jude Children Research Hospital, Memphis, TN, USA

[5]The Jackson Laboratory, Bar Harbor, ME

[6]Eunice Kennedy Shriver National Institute of Child Health and Human Development, Bethesda, MD

[7]Kite Pharma, Santa Monica, CA

* These authors contributed equally to the present work

[#] These authors are co-corresponding authors

Summary (150 words)

Investigating the impact of immune-modulating therapies on mRNA vaccine efficacy remains vital, transcending the immediate context of the COVID-19 pandemic. This study focuses on the differential immune responses to COVID-19 mRNA booster vaccines among healthy volunteers, cancer patients undergoing treatment with immune-checkpoint inhibitors (ICIs), and those treated with the anti-CD20 antibody rituximab. Utilizing RNA sequencing, serology, and interferon-γ release assessment, we charted the temporal dynamics of the immune response in such cohorts. Our findings indicate that ICIs maintain an immune profile similar to that of healthy individuals, whereas treatment with rituximab leads to the impairment of type I interferon response and the upregulation of transcripts pertaining to regulatory T cells, with a global dysregulation of both humoral and cellular immunity. This research deepens our understanding of the sophisticated interplay within the immune system in health and disease states, potentially informing therapeutic strategies across a spectrum of immunological conditions.

Introduction

The advent of mRNA vaccines has represented an instrumental game-changer in the fight against the Coronavirus disease 2019 (COVID-19) pandemic. Specifically, the primary vaccination cycle with BNT162b2 or mRNA-1273 offered a 95% protection against the original SARS-CoV-2 strain in the general population [1,2]. However, this protection wanes after six months, making a third (booster) dose necessary [3]. Cancer patients, being especially at risk, have prompted extensive research into their vaccine-induced immune response [4,5].

Immune perturbagens commonly used in cancer treatment, such as anti-CD20 agents and immune-checkpoint inhibitors (ICIs), exert distinct immunosuppressive and immunostimulatory effects on the host immune system [6,7]. Among cancer patients, those with hematological malignancies undergoing anti-CD20 agents show the lowest seroconversion rate to COVID-19 vaccination. In contrast, treatment with ICIs has been linked with higher seroconversion rates compared to standard cytotoxic chemotherapy, suggesting a potential enhancing effect of immunotherapy on vaccination [8].

Vaccination represents an ideal model for the evaluation of the response mechanisms to a reproducible antigenic stimulation. Indeed, systems vaccinology has shed light on the intricate interplay between innate and adaptive immunity in the physiologic response to mRNA vaccines, revealing distinct response patterns after the first and second dose [9,10]. Notably, Arunachalam *et al.* identified distinct early interferon responses following the first and second dose of the BNT162b2 vaccine, with an enhanced innate immune response, particularly after the second one. This

heightened response is characterized by an increase in $CD14^+$ $CD16^+$ monocytes and antigen presenting cells, which facilitate the crosstalk with B and T cells.

A study by Lee *et al.* on patients with chronic lymphocytic leukemia, using blood RNA-Sequencing (RNA-Seq), revealed an early interferon response akin to that of cancer-free individuals [11]. However, limitations such as low sample size, absence of cancer-free controls, and heterogeneity of treatments and vaccination strategies precluded definitive conclusions.

Overall, the effects of iatrogenic perturbation of the adaptive immunity, whether through B-cell depletion or T-cell stimulation, on the immune response to COVID-19 vaccination in patients with blood and solid cancer, remain largely underexplored.

In this study, we conduct a comprehensive, serial analysis of the immune response to the booster dose of COVID-19 mRNA vaccines by contrasting its effects in healthy individuals and in cancer patients undergoing immune-system-perturbing therapies. In particular, we compare cancer-free volunteers (C-FV) with patients affected by non-Hodgkin lymphoma treated with anti-CD20 agents (rituximab - RTX) and solid tumor patients on ICIs. We explore the evolving phases of vaccine-induced immune response utilizing whole blood RNA-Seq, complemented with multiplex serology and interferon-γ release assessment (IGRA) to evaluate the effectors of humoral and cell-mediated immunity, respectively. Building on our previous research [10], which dissected the transcriptomic temporal dynamics of the immune response to the primary mRNA vaccine cycle, we now focus our RNA-Seq analysis on the early peak responses previously observed after the first and second dose (i.e. 24 hours and 5 days after each dose). Additionally, we broaden our analysis to include assessments of the humoral and cell-mediated immunity at six months post-booster, aiming to evaluate the enduring nature of the vaccine-induced immunity.

In summary, this study provides a comprehensive analysis of the immune response to the COVID-19 mRNA booster vaccine in cancer-free individuals, as well as cancer patients undergoing immune perturbagens such as anti-CD20 agents and ICIs. This analysis aims to delineate the specific impacts of different immune-perturbing treatments on the integrated dynamics and persistence of vaccine-induced immunity, expanding our understanding of immune responses in these distinct patient groups.

Results

Demographics and study design

We collected 214 peripheral blood samples from a total of 44 individuals over an eight-month time span, comprising 22 C-FV, 11 ICI patients, and 11 RTX patients. Clinical characteristics of the study cohorts are reported in **Table 1**, whereas collection and event timelines are depicted in **Supplementary Figure 1**.

All RTX patients were diagnosed with non-Hodgkin lymphoma and were receiving rituximab at the time of enrollment, either as monotherapy (n = 9) or in combination regimens (bendamustine, n = 1 and R-COMP, n =1). The ICI cohort included patients with lung cancer (n = 8), liver cancer (n = 1), urothelial cancer (n = 1), and breast cancer (n = 1), treated with pembrolizumab (n = 9) or atezolizumab (n = 2). The majority of participants (n = 41) received the BNT162 vaccine booster, while three C-FV individuals were administered the mRNA-1273 vaccine.

The C-FV cohort was characterized by a significantly lower median age compared to both ICI patients (adjusted p-value = 0.0036) and RTX patients (adjusted p-value = 0.0021). Extended data, including tumor type and stage, comprehensive therapy details, comorbidities, COVID-19 vaccination history and diagnosis, and sample collection timelines, are provided in **Supplementary Table 1**.

To accurately profile the vaccination response in time, while providing minimal discomfort to the study participants, we utilized an ultra-low volume sampling procedure via fingerpick for both blood RNA-Seq and serological analyses, as previously described [10]. Blood transcriptome was assessed for all participants at baseline (day 0), 24 hours (day 1), and five days (day 5) following the booster dose. Serological profiling was performed at day 0, four weeks (week 4), and six months (month 6) post-booster. For SARS-CoV-2, we tested the reactivity to a stabilized trimer of the Spike protein (S-Trimer), its Receptor Binding Domain (RBD), the Spike subunit S1 (S1), and the Nucleocapsid (Nucleo) and Envelope (Env) proteins. Reactivity to the S1 antigens of various human coronaviruses (hCoVs), including SARS-CoV, MERS, HCoV-229E, HCoV-NL63, HCoV-HUK1, and HCoV-OC43, was also tested. The seroreactivity to these antigens was quantified by measuring the Binding Antigen Index (BAI) increment for IgM, total IgG, and the different subclasses of IgG (IgG1, IgG2, IgG3), as well as IgA (IgA1, IgA2). The cell-mediated immune response to the vaccine was assessed using IGRA in a subset of 12 C-FV, 4 ICI, and 8 RTX at day 0, day 5, week 4, and month 6. An interferon-γ concentration of 200 mUI/mL after stimulation with native SARS-CoV-2 S1 was set as the threshold for positive response, while lower values were considered as borderline or negative. A detailed description of the analyses is provided in the Methods.

Serological profiling of C-FV identifies distinct patterns of humoral response to SARS-CoV-2 at four week and six months from vaccination

We assessed the humoral response to the COVID-19 booster dose by performing a comprehensive evaluation of antibodies directed against various antigens of SARS-CoV-2 and the S1 of several hCoVs. To evaluate vaccination response, we used a

mixed-effects model, without and with intervening COVID-19 diagnosis as a covariate adjustment. This allowed us to quantify the variation of BAI to reflect both temporal antibody level changes (BAI_t) and the association of such variation with COVID-19 diagnosis ($BAI_{COVID\text{-}19}$).

In the C-FV group, the COVID-19 booster administration resulted in a notable increase in vaccine-targeted antibodies at week 4 (**Figure 1**), particularly total IgG targeting RBD (BAI_t = 8.92, false discovery rate (FDR) = 1.17 10^{-6}), S-Trimer (BAI_t = 14.06, FDR = 7.62 10^{-7}), and S1 (BAI_t = 20.39, FDR = 7.62 10^{-7}). No significant response to Nucleo was detected, except in one individual with prior virus exposure who showed a marked increase in anti-Nucleo total IgG and IgG2 levels (**Figure 1A**). A moderate increment in anti-Env total IgG was noted (BAI_t = 0.022, FDR = 1.4 10^{-4}). At month 6, a significant rise in antibodies associated with natural infection was detected, such as anti-Env IgM (BAI_t = 0.037, FDR = 0.005) and total IgG (BAI_t = 0.23, FDR = 0.00025), as well as anti-Nucleo IgM (BAI_t = 0.049, FDR = 0.00062), regardless of COVID-19 diagnosis. Most vaccine-targeted antibodies showed further increases compared to week 4 (**Supplementary Table 2**).

Considering hCoVs, a pronounced cross-reaction with the SARS-CoV Spike protein was observed following the booster administration, as evidenced by a substantial augmentation in anti-S1 total IgG for SARS-CoV at week 4 (BAI_t = 22.47, FDR = 4.32 10^{-5}; **Supplementary Figure 2**), corroborating prior findings [10]. At month 6, there was a significant enhancement in anti-S1 IgM and total IgG for MERS (FDR of 0.0097 and 0.0073), HCoV-229E (FDR of 0.0031 and 3.34 10^{-7}), HCoV-NL63 (FDR of 0.01383 and 0.0009), HCoV-HUK1 (FDR of 0.0092 and 0.0006), and HCoV-OC43 (FDR of 0.015 and 0.0012; **Supplementary Figure 2**; **Supplementary Table 3**). Anti-S1 IgM of hCoVs assessed at month 6 significantly correlated with anti-Env and

anti-Nucleo IgM of SARS-CoV-2, independently of intercurrent COVID-19 diagnosis (**Supplementary Figure 3**). A similar trend was noted for SARS-CoV-2 anti-RBD IgM. Notably, SARS-CoV-2 anti-S-Trimer IgM correlated with anti-S1 IgM of hCoVs only in subjects without a diagnosis of COVID-19, whereas SARS-CoV-2 anti-S1 IgM showed correlation specifically in infected subjects.

Overall, the COVID-19 booster effectively enhances humoral response against Spike protein antigens, with no observed effect on anti-Env and anti-Nucleo antibodies, aligning with existing evidence [10]. Vaccine-targeted antibodies remain persistently elevated six months post-booster. While this suggests that the booster dose elicits long-lasting humoral immunity to the virus, the significant rise in infection-associated antibodies at month 6 implies a role of natural infection in stimulating and maintaining a polyfunctional humoral response to the virus. Indeed, seroconversion for Env and Nucleo antigens in most C-FV at month 6, irrespective of COVID-19 diagnosis, likely reflects asymptomatic COVID-19 cases or, intriguingly, infection with cross-reactive coronaviruses, as indicated by the significant positive correlation of SARS-CoV-2 IgMs with anti-S1 IgMs of hCoVs six months after vaccination. The lifting of FFP2 and surgical mask mandates in public places and on public transportation by the Italian Government in the period between week 4 and month 6 may have influenced these findings. Taken together, our data suggest that multiple factors contribute to the development of a comprehensive and long-lasting humoral immunity to SARS-CoV-2, with infection by SARS-CoV-2 or other hCoVs possibly acting as a natural booster in previously vaccinated subjects.

Humoral immune response to COVID-19 booster is preserved in ICI patients, but severely impaired in RTX cases

In ICI patients, the humoral response to the COVID-19 booster dose mirrored that of the C-FV group, exhibiting a pronounced increase in vaccine-specific antibodies at week 4. This included a rise in total IgG targeting RBD (BAI_t = 4.75, FDR = 0.038, S-Trimer (BAI_t = 8.19, FDR = 0.038), and S1 (BAI_t = 11.90, FDR = 0.038 3.8 10^{-2}). Similarly to C-FV individuals, ICI patients demonstrated a significant increase in infection-associated antibodies at month 6, including anti-Env IgM (BAI_t = 0.016, FDR = 0.038) and total IgG (BAI_t = 0.13, FDR = 0.013) and anti-Nucleo IgM (BAI_t = 0.039, FDR = 0.089; **Supplementary Table 2**).

In contrast, RTX patients did not mount a humoral response to the booster dose, as shown by negligible changes compared to baseline in anti-RBD total IgG (BAI_t = -1.21, FDR = 0.70), anti-S-Trimer total IgG (BAI_t = -1.60, FDR = 0.70), and anti-S1 total IgG (BAI_t = -2.61, FDR = 0.70) at week 4. However, at month 6, an increase in vaccine-targeted antibodies associated with intercurrent clinically manifest COVID-19 was observed, (anti-RBD total IgG $BAI_{COVID\text{-}19}$ = 5.77, FDR = 0.074; anti-S-Trimer total IgG $BAI_{COVID\text{-}19}$ = 13.08, FDR = 0.017; anti-S1 total IgG $BAI_{COVID\text{-}19}$ = 13.32, FDR = 0.062; **Supplementary Table 1**). Indeed, three RTX patients were diagnosed with COVID-19 during the study period. Intriguingly, only patients UPN41 and UPN43, who contracted COVID-19 shortly after vaccination (12 and 14 days, respectively), mimicking the temporal proximity of the two vaccine doses of primacy vaccination cycle, developed a humoral response towards SARS-CoV-2 (**Figure 1C**). In contrast, patient UPN49, diagnosed with COVID-19 at 44 days post-booster, showed no response at month 6. While anecdotal, this finding suggests that a complete two-dose re-vaccination cycle may achieve higher seroconversion rates than a single booster dose in this subset of immunocompromised patients.

The cell-mediated immunity against SARS-CoV-2 is impaired in RTX patients and is temporarily restored by the booster dose of COVID-19 vaccine

Next, we evaluated the cell-mediated immune response to the booster dose using an IGRA assay to measure interferon-γ release from T-cells upon exposure to SARS-CoV-2 S1. C-FV group and patients in the ICI cohort showed no significant differences, all maintaining positive baseline IGRA results across all post-booster time points (**Figure 1D, Supplementary Table 4**).

Conversely, RTX patients displayed weaker cell-mediated responses than C-FV at day 0 and at week 4, with only 37.5% and 33.3% testing IGRA-positive, compared to 83.3% and 100% in C-FV (p-values of 0.062 and 0.0049, respectively). Of note, the cell-mediated response in such cohort was restored at day 5 and at month 6 after vaccination with 75% and 85.7% showing positive IGRA results.

This pattern in RTX patients suggests that prolonged rituximab exposure adversely affects cell-mediated immunity to SARS-CoV-2, likely due to disrupted B and T-cell interaction or, potentially, direct effects of rituximab on T cells [7]. Although the booster temporarily restores cell-mediated immunity, a persistent depletion of CD20+ cells may hinder, at least partially, a durable and efficient T cell-mediated response. The eventual recovery of this response at month 6, possibly influenced by infection by SARS-CoV-2 or other hCoVs (as noted for humoral responses), suggests reversibility and potential enhancement of cell-mediated immunity even in RTX patients through repeated antigen exposure.

Modular analysis of COVID-19 booster reveals orchestrated immune response with early interferon spike followed by activation of adaptive immunity.

To investigate the early dynamics of the immune response to the COVID-19 booster vaccination, we conducted a time-course analysis of the whole peripheral blood transcriptome through RNA-seq, applying the modular approach originally established by Chaussabel *et al.* and implemented in the BloodGen3 package [12–14]. This method involves categorizing RNA transcripts into 384 fixed transcriptional modules, co-clustering across 16 different immunological and physiological states and further consolidated in 38 aggregates for functional annotation. This framework enables the analysis of transcriptional module profiles at both group- and single-sample level, facilitating the identification of phenotype-specific patterns and broader insights into variations between different groups. The overall response to vaccination within each study cohort was assessed by using the group-level comparison (**Figure 2**). The Shannon entropy index (SEI) was used to express transcriptomic diversity of modular repertoire functions at each contrast [15]. We first profiled the transcriptomic response to COVID-19 booster dose in the C-FV cohort by contrasting module abundance on days 1 and 5 against the baseline on day 0, observing a response involving 21 and 9 modules, respectively. On day 1, we observed a pronounced increase in six modules linked to interferon response and one module related to inflammation (M10.1, M15.86, M13.17, M15.64, M15.127, and M8.3 aggregate A28 and M13.12, aggregate A35 respectively, SEI = 0.79). Simultaneously, we noted a transient decrease in several modules associated with cytotoxic lymphocytes (M9.1 and M13.21), T cells (M15.38), cell cycle (M14.31, M15.73), and gene transcription (M14.17 and M14.69; SEI = 1.37), aligning with the established physiologic response to the BNT162b1 vaccine [16]. By day 5, we observed a rise in 9 modules, including transcripts associated with effectors of adaptive immunity such as plasma cells (M12.15, aggregate A27) and T cells (M12.6, M15.98, and M15.38, aggregate A1

and A6; SEI = 1.21). The comparison between day 5 and day 1 showed a polyfunctional response involving 92 modules, with a widespread upregulation of aggregates A1, A2, A3, and A5 (SEI = 2.19). These aggregates are associated with effectors of adaptive immunity and cell proliferation or activation, such as cytotoxic lymphocytes (M9.1 and M13.21), lymphocytes (M13.27, M16.78, M13.18, M15.24), T cells (M14.42, M15.38, M12.6, M15.98, M16.3, M15.33), cell cycle (M14.31, M12.3, M15.73), cell death (M15.29, M15.23, M15.49), gene transcription (M13.2, M14.71, M14.4, M14.34, M14.17, M14.23, M16.36, M15.21, M15.8, M15.3, M13.13, M14.69), mitochondrial stress/proteasome (M15.79), oxidative phosphorylation (M14.63), protein modification (M16.50, M16.99, M15.92, M16.13, M15.44, M12.1, M15.31, M12.5) and protein synthesis (M14.75, M11.1, M15.51, M13.4, M16.73, M10.2, M16.68, M16.56, M14.44). In concomitance with such widespread activation of immune response and cell machinery, modules associated with interferon and inflammation were downregulated (SEI = 1.76; **Figure 2**). Response values for each module at each time point contrast are reported in **Supplementary Table 5**.

To further explore the functional trajectories of COVID-19 booster, modules sharing the same functional annotation in Bloodgen3 were incorporated and assessed in a correlation matrix (**Figure 2C**). Notably, interferon modules had a significant positive correlation with plasma cells and inflammation and were inversely correlated with cytotoxic lymphocytes, lymphocytes, and TGF-beta. Signatures associated with cell machinery processes (i.e. cell cycle, cell death, gene transcription, oxidative phosphorylation, mitochondrial stress/proteasome, protein modification and phosphorylation) clustered with signatures of either innate (i.e. monocytes, complement, antigen presentation) or adaptive (i.e. B cells, T cells, lymphocytes)

immunity. In parallel, we observed a further cluster of signatures associated with acute inflammation (i.e. neutrophils, inflammation, cytokines/chemokines).

Taken together, these findings indicate that the COVID-19 booster vaccination triggers an immediate, transient interferon surge, driving an orchestrated, polyfunctional adjustment of adaptive and innate immunity pathways.

Comparative transcriptomic responses to COVID-19 booster reveal distinct patterns and functional dynamics in ICI and RTX patients.

We next assessed the transcriptomic response to COVID-19 booster in ICI and RTX patients (**Supplementary Figure 4)**. The magnitude of modular response, in terms of absolute number of upregulated or downregulated modules, and the transcriptomic diversity of modular repertoire functions, in terms of SEI, were compared with C-FV at each time point contrast through Fisher's exact test and Hutcheson test, respectively.

After booster administration, ICI patients showed a day 1-transcriptomic response similar to C-FV individuals with upregulation in 8 modules (p-value = 1) and a predominant spike of interferons (SEI = 1.15, p-value = 0.18; **Figure 3**) while having, in contrast to C-FV, only one downregulated module (p-value = 0.0008), associated with protein synthesis (M13.28). On day 5, ICI patients displayed upregulation in 20 modules (p-value = 0.057) including transcripts linked to cell cycle (M14.64 and M14.31), plasma cells (M15.110, and M15.12), platelets (M14.81, and M15.45), monocytes (M15.7), T cells (M12.6), and gene transcription (M14.55; SEI = 1.95, p-value 0.005; **Supplementary Figure 5A**). Comparative analysis of module abundance between day 5 and day 1 revealed a response of 23 modules (p-value = $1.51\ 10^{-12}$) involving functions related to the adaptive immunity and cell proliferation,

including cytotoxic lymphocytes (M13.21), cell cycle (M14.64, M16.104), protein synthesis and modification (M14.58, M13.28, M14.13), T cells (M15.34), and plasma cells (M12.15; SEI = 1.93, p-value = 0.14; **Supplementary Figure 5B**). Modules associated with interferon and inflammation were found deregulated (SEI = 1.54, p-value = 0.19), aligning with C-FV.

RTX patients exhibited a distinct early immune perturbation, with the upregulation of 45 modules occurring at day 1 (p-value = $2.58\ 10^{-8}$), including transcripts associated with oxidative phosphorylation (M14.13), gene transcription (M14.34, M15.126, M14.67), cell adhesion (M15.56), protein modification (M15.92,M15.44, M14.14) and phosphorylation (M13.19, M16.84), oxidative stress (M16.107), and inflammation (M15.37, M14.19, M13.12, and M14.24; SEI = 1.84, p-value = 0.003; **Figure 3**). Notably, 22 of the 45 upregulated modules were not functionally annotated in Bloodgen3 (TBD). We therefore performed overrepresentation analysis of transcripts included in such modules by using MSigDB [17,18], observing a significant association with two signatures related to differentiation of T cells towards regulatory T cells (GSE42021_TREG_VS_TCONV_PLN_UP, FDR = 0.047; GSE42021_CD24LO_TREG_VS_CD24LO_TCONV_THYMUS_DN, FDR = 0.047; **Figure 3D**). On day 5, there was an upregulation of 56 modules (p-value = $4.31\ 10^{-10}$) pertaining to both adaptive and innate immunity, including T cells (M15.98), neutrophils (M14.28), inflammation (M14.19, M14.50, and M14.24), oxidative stress (M16.107), and B cells (M16.95), along with modules associated with cell proliferation and death (M14.54 and M16.97) and protein machinery (M14.14, M15.44, M12.1, M16.84, M13.10, and M16.11; SEI = 1.70, p-value = 0.03; **Supplementary Figure 5A**). Thirty-three of 56 modules were TBD, but no significant associations with MSigDB signatures were observed. The differential module

response assessment at day 5 vs. day 1 highlighted a positive response involving only 6 modules (p-value = 2.88 10^{-23}), with the upregulation of two modules linked to platelets (M16.109 and M10.3), two to prostaglandins and prostanoids (M16.64, M15.102), and one to the cell cycle (M14.39; SEI = 1.56, p-value = 0.001; **Supplementary Figure 5B**). Four modules, including two associated with interferon (M10.1, M15.86) and one associated with cell cycle (M13.20), were found deregulated (SEI = 1.04, p-value = 0.005).

Overall, ICI's response aligned with that of C-FV, with a more pronounced day 5-response in terms of both magnitude and diversity. Conversely, RTX patients exhibited a markedly divergent phenotype of response from C-FV, as highlighted by the transcriptional entropy occurring on both day 1 and day 5 compared to day 0 and the modest response occurring between day 5 and day 1, denoting an uncoordinated response to vaccination.

Type I interferon response to COVID-19 booster is blunted in RTX patients.

Despite the different response patterns and treatment conditions, all study cohorts exhibited a notable interferon peak on day 1 post vaccination. Therefore, we set to profile in greater detail the response dynamics of aggregate A28 across the different groups (**Figure 4**). To this aim, we used two distinct signatures identified in our previous work by performing hierarchical clustering on the six interferon modules of aggregate A28 after the first and second dose of COVID-19 vaccine [10]. Of these, signature A28/S1 includes modules M8.3, M10.1, and M15.127, while signature A28/S2 includes modules M15.64, M13.17, and M15.86.

By implementing a mixed effect model to account for the response of each signature between day 1 and day 0, we identified A28/S1 as significantly increased in C-FV (p-

value = 7.88 10^{-14}) and ICI patients (p-value = 8.65 10^{-13}). Notably, RTX patients did not mount a significant response in the A28/S1 signature (p-value = 0.151). In particular, of the A28/S1 modules, the response of M8.3 (p-value = 0.506) and M15.127 (p-value = 0.304) were depleted, while the response of M10.1 was preserved (p-value = 6.66 10^{-6}). A28/S2, along with each module included in the signature, was found significantly increased in all cohorts.

A28/S1 modules encompass genes from the oligoadenylate synthetase family (*OAS1*, *OAS2*, *OAS3*, *OASL*), interferon-induced protein family (*IFI6*, *IFI27*, *IFI35*, *IFI44*, and *IFI44L*), and interferon-induced protein with tetratricopeptide repeats family (*IFIT1*, *IFIT3*, and *IFIT5*), canonically induced by type I interferon. Modules of signature A28/S2 include transcription factors *IRF9* and *STAT2*, along with nuclear antigen family members *SP100*, *SP110*, and *SP140*, associated with interferon-γ signaling pathway.

Such results indicate a substantial impairment of the type I interferon response in RTX patients, a key component in the innate response to viruses and the cross-talk between innate and adaptive immunity [19,20]. This impairment in the type I interferon signaling may underpin the uncoordinated response to the COVID-19 booster observed for such patients, resulting in a dysfunctional response to the vaccine with a switch of T cells towards a regulatory phenotype [21].

Immune cell deconvolution of blood transcripts reveals depletion of antigen presenting cells and B cells in RTX patients after booster administration

In order to evaluate changes in blood cell composition after booster administration across the different study cohorts, we performed immune cell deconvolution on blood RNA-seq. To this aim, multiple deconvolution methods were assessed. CIBERSORT

was identified as the method that showed the highest correlation with peripheral blood counts performed according to clinical practice concurrently with RNA-seq and was therefore chosen for further analysis (**Supplementary figure 8**).

In the C-FV cohort, we observed an increase of plasma cell and memory B cell on day 1 and day 5 compared to day 0 (**Figure 5, Supplementary figure 8**). Moreover, an initial increase in monocytes and activated dendritic cells was noted (**Figure 5, Supplementary figure 8**), in line with the available literature [9]. $CD8^+$ T cells exhibited an upregulation on day 5 following a transient decrease on day 1.

Similar patterns were noted in ICI patients, where blood cell deconvolution revealed a markedly pronounced upregulation of resting NK cells and M1-differentiating monocytes on day 1.

Of special interest, RTX patients displayed a suppression of antigen presenting cells, such as activated dendritic cells and M1-differentiating monocytes, as well as B cells on both day 1 and day 5. Across all study cohorts, a progressive upregulation of $CD4^+$ T activated memory cells was observed.

Discussion

In the present study, we conduct the first comprehensive characterization of the early and late phases of the immune response to consistently reproducible antigenic stimulation in patients treated with anti-CD20 agents and ICIs, thus bridging a knowledge gap regarding the biological determinants that underpin their immunosuppressive and immunostimulatory effects. Specifically, we used the COVID-19 booster as a model to assess the immune response in two distinct cohorts of patients with blood and solid cancers undergoing active treatment with rituximab and ICIs. To this aim, we opted for a system-scale approach based on the

analysis of co-dependent transcriptional networks identified by Altman *et al*. [13]. Differently from traditional methods based on feature selection or dimension reduction, this approach considers the complex interdependence of variables in biological systems, allowing for a more informative evaluation of transcriptional changes that would not be detected if considering single genes as independent variables [22].

Our initial step was to characterize the immune response to COVID-19 vaccination in individuals with good overall health (C-FV). The booster dose of vaccine in the C-FV cohort led to an early isolated interferon response resembling the one observed after the first dose [10]. This finding confirms that the temporal proximity of the two vaccine doses administered within the primary cycle is critical to elicit the polyfunctional innate response seen after the second dose [10], even in individuals who have completed the primary vaccination cycle. The early isolated interferon peak following the booster dose of vaccine likely acts as a trigger of immune memory mechanisms involving cells of the adaptive immunity primed by the first and second doses [23]. Such transcriptional response is then associated with the restoration of SARS-CoV-2 humoral immunity, as highlighted by the marked increase of vaccine-targeted antibodies after four weeks.

Similarly to C-FV, ICI patients showed a preserved humoral and cell-mediated immune response to COVID-19 booster, while RTX patients were heavily immunosuppressed. Blood transcriptome dynamics in ICI patients resembled that of C-FV, with subtle differences consistent with a state of ongoing immune stimulation, including the absent downregulation of immune modules on day 1, observed for the C-FV, and an enhanced response on day 5. The marked upregulation of NK cells observed by cell deconvolution on day 1 aligns with data reported by Nelli *et al*. [24]

and, together with the pronounced response of M1-differentiating monocytes, further supports such hypothesis. No other unusual findings were observed in the dynamics of humoral, cellular and transcriptomic response of ICI patients, supporting the efficacy and, likely, the safety of the concomitant administration of immunotherapy and COVID-19 vaccines.

On the other hand, the transcriptional profile of RTX patients was characterized by an overall immune dysfunction, denoted by the state of transcriptomic perturbation observed on both days 1 and 5, coupled with a substantial deficit in the type I interferon response and the upregulation of transcripts associated with differentiation of regulatory T cells. Type I interferon plays a critical role in the innate response to viruses, including SARS-CoV-2 [19], and is implicated in the crosstalk between antigen presenting cells and B cells, enhancing the humoral immunity by promoting B cell differentiation and isotype switching [20]. Consistently, immune cell deconvolution of blood transcripts showed a concomitant depletion of antigen presenting cells and B cells in RTX patients. Notably, Graalmann *et al*. described a type I interferon-dependent mechanism in the impairment of $CD8^+$ T cell responses following B-cell depletion in murine models infected with modified vaccinia virus Ankara [25]. In parallel, the administration of rituximab has been associated with expansion of Tregs, likely as a direct effect of B cell depletion [7]. Of interest, depletion of Tregs has been associated with an enhanced response to COVID-19 vaccination, suggesting an inverse correlation with vaccine efficacy [26].

The humoral and cell-mediated responses assessed six months after the booster dose may have been influenced by intercurrent immune stimulations. In such regard, while it is unclear whether pre-existing hCoVs immunoglobulins confer protection towards COVID-19, cross-reaction between SARS-CoV-2 and hCoVs has been

documented [27,28]. Since SARS-CoV-2 infection results in increased titers of hCoVs antibodies [29], infections by common hCoVs may in turn enhance the humoral immunity towards SARS-CoV-2, providing indirect protection by acting as a natural booster of the host immune response.

Our work has several limitations. The small size of our sample highlights the exploratory nature of our study, particularly in assessing cell-mediated immunity. This limitation restricted our ability to evaluate and adjust for possible confounding factors like age and comorbidities. In our cohort, cancer patients were generally older and had more comorbidities than those in the C-FV group. Despite recognizing this limitation, the rapid deployment of the booster dose in Italy necessitated swift action within a very limited timeframe, which explains our lower participant numbers. Additionally, our assessment of humoral and cell-mediated immunity focused on the original SARS-CoV-2 variant without accounting for the emergence of new variants of concern. Nevertheless, this should not detract from the significance of our findings. Our goal was to assess the framework of immune response following a reliable, reproducible immune stimulus in patients treated with specific immune perturbagens. As such, our work may in principle be confirmed by downstream studies conducted during future vaccination campaigns. Finally, blood cell decomposition was performed computationally on blood RNA and can therefore reflect changes in the transcriptional activity of cells rather than in the actual blood composition. Nonetheless, changes in blood cell deconvolution values can be indicative of underlying changes in cell function or state, and may still be relevant to understanding the response to various conditions or treatments in different groups. Indeed, the increase of NK cell and M1-differentiating monocytes in ICI patients and the decrease of antigen presenting cells in rituximab patients offer intriguing and

biologically coherent insights into the interplay amongst the various actors of innate and adaptive immunity and its alterations in non-physiological conditions.

In conclusion, our study represents a significant advancement in understanding the immune responses to COVID-19 vaccination in patients undergoing treatment with immune-perturbing agents such as RTX and ICIs. By employing a system-scale analysis of transcriptional networks, we were able to uncover intricate details of the immune response that traditional methods might overlook. Our findings reveal that the early interferon response plays a pivotal cross-talk role in triggering immune memory mechanisms, crucial for the restoration of SARS-CoV-2 humoral immunity. The preserved humoral and cell-mediated responses in ICI patients, contrasted with the immune dysfunction in RTX patients, highlight the potential impact of these treatments on vaccine efficacy. Moreover, our work points to the importance of type I interferon responses and the regulatory role of T cells in shaping the B-mediated immune response to vaccination. Likewise, our findings stress the relevance of a functional B-mediated response to elicit an orchestrated innate and adoptive T-cell mediated immunity. Our efforts lay the groundwork for future studies aimed at optimizing vaccination strategies and improving outcomes in vulnerable populations, as well as understanding better how B and T cells interact in coordinating the immune response in physiological and pathological states. Further research is needed to validate our results in larger cohorts and against emerging variants of concern, but our study marks a crucial step towards understanding the biological determinants of immunosuppressive and immunostimulatory effects of cancer therapies on vaccine-induced immunity.

Methods

Patient recruitment

Patients with solid or blood cancer were recruited at the Hematology, Oncology, and Internal Medicine units of IRCCS Ospedale Policlinico San Martino (HSM - Genoa, Italy). C-FV were recruited amongst health care workers at University of Genoa and HSM, as well as external volunteers in good general health conditions.

All subjects were scheduled to receive the third dose of COVID-19 mRNA vaccine, either BNT162b2 or mRNA-1273. RTX patients were considered eligible for the study if treated with rituximab within the previous nine months. ICI patients were considered eligible if undergoing active treatment with ICI at the moment of recruitment.

All subjects were assessed using the following exclusion criteria: symptomatic infection of proven or suspect viral or bacterial origin in the previous 8 weeks (paraneoplastic fever was not considered an exclusion criteria); major trauma or surgery in the previous 8 weeks; hereditary immunodeficiency; HIV infection; active immunologic disorders (autoimmune disease, active allergic disease or undergoing chronic treatment); treatment with immunosuppressive drugs not for cancer treatment; acute or chronic end-stage liver disease; acute or chronic end-stage (stage III-IV) kidney disease.

Study design

Capillary blood samples were collected from all subjects at day 0, day 1, day 5, week 4 and month 6 after vaccination. Peripheral venous blood samples were collected

from a subset of patients and C-FV at day 0, day 5, week 4, and month 6. No patient received cancer treatment between day 0 and day 5. Whole blood transcriptome sequencing was performed on capillary blood samples collected at day 0, day 1, and day 5. Multiplex SARS-CoV-2 and hCoV serology was performed on capillary blood samples collected at day 0, week 4, and month 6. Cell-mediated immunity to SARS-CoV-2 was assessed through interferon-γ release assay (IGRA) on peripheral venous blood samples collected at day 0, day 5, week 4, and month 6. Intercurrent diagnoses of COVID-19 were assessed at each appointment scheduled per study protocol. Subjects were considered as diagnosed with COVID-19 in case of positive molecular or antigenic nasopharyngeal swab recorded in HSM or reported at the moment of sample collection.

Sample collection

For whole blood RNA-seq, we collected 50 µL of capillary blood through finger-puncture using the capillary blood and tube assembly GK100 (Kabe Labortechnik, Nümbrecht, Germany), previously aliquoted with 100 µL of Tempus™ Blood RNA Tubes stabilizing reagent [30]. GK100 tubes were then labeled and stored at -20°C in a dedicated freezer (Beko). For multiplex SARS-CoV-2 and HCoV serology, we collected 20 µL of capillary blood through finger-puncture using Mitra® fingersticks (Neoteryx, Torrance, CA, USA), subsequently stored at room temperature. Peripheral venous blood samples (~5 mL) for IGRA were collected through peripheral venipuncture in one heparinized Vacuette ® tube.

Whole blood RNA extraction, quality check, and library preparation

Total RNA was extracted from GK100 tubes using the Tempus™ Spin RNA Isolation Kit Protocol with minor modifications. RNA quality check was performed using the RNA ScreenTape (Agilent) on a TapeStation 2200 device (Agilent). RNA samples with RNA integrity number above 7 were considered of good quality. Up to 200 ng of input RNA were used to prepare the libraries for 3' mRNA-Seq using the QuantSeq 3' mRNA-Seq Library Prep Kit for Illumina FWD with UDI 12 nt Unique Dual Indexing (Lexogen). Libraries were outsourced to Lexogen for sequencing at 1x75 bp length, 8 megareads per sample on a NextSeq1000 sequencer.

Assessment of cell-mediated immune response to vaccination.

The cell-mediated immunity to SARS-CoV-2 was evaluated through IGRA using a commercially available kit (Quan-T-cell Euroimmun™). Fresh whole blood samples were aliquoted in three different tubes respectively with a) no T-cell stimulation for the assessment of the interferon-γ background; b) specific T-cell stimulation using SARS-CoV-2 S1; c) nonspecific T-cell stimulation by means of a mitogen. All samples were stimulated within five hours from collection as per manufacturer's instructions. After the incubation, each tube was centrifuged to obtain stimulated heparinized plasma. The concentration of interferon-γ was subsequently assessed using the enzyme-linked immunosorbent assay (ELISA) provided by the manufacturer. We used the recommended thresholds of interferon-γ concentration to determine negative, borderline, and positive results, respectively set at < 100 mUI/mL, 100-200 mUI/mL, > 200 mUI/mL.

Computational methods

Assessment of binding antibody index changes

The matrix of raw antibody indices was processed within the R environment using custom scripts. First, the fold-change for each time point against the relative baseline for each antibody was assessed at individual sample level. To estimate group variations compared to the basal level of each antibody, we implemented a mixed-effects model, accounting for paired samples and COVID-19 diagnosis intervening between samplings. The fixed model coefficients were extracted and used as the unitary increment of the antibody index as a function of time (BAI_t) and COVID-19 diagnosis ($BAI_{COVID\text{-}19}$). The correlation between SARS-CoV-2 and hCoVs antibodies was assessed with Spearman's rank correlation coefficients using the raw antibody index matrix.

Alignment of 3' mRNA-Seq, quality check, and processing

FASTQ files were processed through the QuantSeq 3' mRNA-Seq Integrated Data Analysis Pipelines on the Bluebee® Genomics Platform. Using the QuantSeq FWD analysis pipeline, raw data were aligned by the STAR v2.5.2a to human genome GRCh38/hg38 (Ensembl release 77, August 2014). QC was performed into two steps, first on the raw counts using FASTQC for a preliminary report of sequencing results and trimming step, then using RSEQC for evaluation of distribution of the reads on the annotation features. Gene counts were estimated by HTSeq-count v0.6.0 and annotated using the Ensembl v77 GTF. All downstream analyses were performed in R. Raw counts were normalized by dividing for sample-specific size factors using the DESeq2 package. RNA-seq data are deposited in [Indicate Repository], together with descriptive information about the overall study and individual samples, with accession ID.

Immune modular repertoire analysis.

Normalized transcriptional levels were aggregated using a prespecified set of 382 transcriptional modules as described in detail in [13,14], using the BloodGen3Module R package. In brief, based on the weighted clustering networks of co-expressed transcripts derived from 16 blood samples, a repertoire of immune modules was identified. Downstream analysis and visualization were performed using custom R scripts based on DESeq2, ggplot2, and ComplexHeatmap. The workflow started with annotating a normalized expression matrix with immune functionals modules, then differential expression was assessed and eventually the immune response was calculated. The immune response is quantified with two different approaches, namely “group comparison”, i.e. the proportion of constitutively expressed genes whose abundance levels differ significantly between two groups, or as “individual comparison”, defined as the proportion of constitutively expressed genes whose abundance levels differ significantly for the same individual compared to a reference point. The values range from -100% to 100%, according to the proportion of decreased or increased constitutive transcripts. The main steps for the group comparison are: a) estimate fold-change variation and p values from the mixed effect model for each gene, b) calculate number of genes belonging to the same module with positive or negative trends ($|logFC| > 1.5$, p value < 0.05), c) if the number of genes of the same module with a positive trend is greater than the number of genes with a negative trend, a positive response is assigned to the module, otherwise a negative response is attributed to the module. The response rate is calculated as the number of significant genes, considering the direction of the response, divided by the total number of genes of a given module. The main steps for the individual sample level comparison are: a) estimate fold-change of a given gene of a given sample

considering as reference the average value of the same gene across a set of control samples, b) calculate the difference in terms of normalized counts between a given gene of a given sample against the average normalized counts of the same gene across a set of control samples, c) calculate number of genes belonging to the same module with positive or negative trends (|logFC| > 1.5, |DIFF| > 20), and d) if the number of genes of the same module with a positive trend is greater than the number of genes with a negative trend, a positive response is assigned to the module, otherwise a negative response is attributed to the module, in line with group comparison. By default, to enhance interpretability, only the strongest direction is displayed, with red shades depicting an increment whereas blue palette describing a decrease in the response. For the “group comparison”, we modified the BloodGen3 approach, implementing a linear mixed-effects model (lme4 package) that accounts for the paired nature of the design of the present study. The Blood3GenModule was also used to visualize the results for both group comparison and individual comparison analyses. As a quantitative measurement of the level of complexity of modular responses, we adopted the Shannon index, computed as the measure of diversity of module repertoire functions upregulated or downregulated at each time point contrast in the different study cohorts. SEIs were calculated using the ecolTest package and compared through multiple Hutcheson t-tests.

Characterization of TBD modules in RTX patients.

Characterization of genes associated to TBD modules upregulated in RTX patients were determined by over-representation analysis using the clusterProfiler package with default settings [31,32]. The C7 (version 7.4) immune signature collection from the MSigDB portal was adopted for annotation [17,18].

Characterization of the day 1 interferon response.

Modules of the aggregate A28 and signatures A28/S1 and A28/S2 were evaluated leveraging a mixed effect model, accounting for same-case sample pairing, measuring the temporal changes of response between day 1 and day 0 for each study cohort.

Immune cell type in-silico deconvolution

To perform immune cell deconvolution on blood transcripts we assessed MCP counter, Epic, Quantiseq, Xcell, CIBERSORT, CIBERSORT absolute, and Abis, comparing neutrophil signatures assessed on blood RNA with paired neutrophil percentages in peripheral blood counts performed per clinical practice in a subset of 15 patients with same-day WBC and RNA-seq measurements. Neutrophils were selected as the benchmark for such comparison, being the immune subpopulation available for all deconvolution methods. The CIBERSORT algorithm was selected as the best performing one for downstream analyses (immunedeconv R package with defaults options).

References

1. Polack FP, Thomas SJ, Kitchin N, Absalon J, Gurtman A, Lockhart S, et al. Safety and Efficacy of the BNT162b2 mRNA Covid-19 Vaccine. N Engl J Med. 2020;383: 2603–2615. doi:10.1056/NEJMoa2034577

2. Baden LR, El Sahly HM, Essink B, Kotloff K, Frey S, Novak R, et al. Efficacy and Safety of the mRNA-1273 SARS-CoV-2 Vaccine. N Engl J Med. 2021;384: 403–416. doi:10.1056/NEJMoa2035389

3. Tartof SY, Slezak JM, Fischer H, Hong V, Ackerson BK, Ranasinghe ON, et al. Effectiveness of mRNA BNT162b2 COVID-19 vaccine up to 6 months in a large integrated health system in the USA: a retrospective cohort study. Lancet. 2021;398: 1407–1416. doi:10.1016/S0140-6736(21)02183-8

4. Al Hajji Y, Taylor H, Starkey T, Lee LYW, Tilby M. Antibody response to a third booster dose of SARS-CoV-2 vaccination in adults with haematological and solid cancer: a systematic review. Br J Cancer. 2022;127: 1827–1836. doi:10.1038/s41416-022-01951-y

5. Fendler A, de Vries EGE, GeurtsvanKessel CH, Haanen JB, Wörmann B, Turajlic S, et al. COVID-19 vaccines in patients with cancer: immunogenicity, efficacy and safety. Nat Rev Clin Oncol. 2022;19: 385–401. doi:10.1038/s41571-022-00610-8

6. Bagchi S, Yuan R, Engleman EG. Immune Checkpoint Inhibitors for the Treatment of Cancer: Clinical Impact and Mechanisms of Response and Resistance. Annu Rev Pathol. 2021;16: 223–249. doi:10.1146/annurev-pathol-042020-042741

7. Avivi I, Stroopinsky D, Katz T. Anti-CD20 monoclonal antibodies: beyond B-cells. Blood Rev. 2013;27: 217–223. doi:10.1016/j.blre.2013.07.002

8. Brest P, Mograbi B, Hofman P, Milano G. COVID-19 vaccination and cancer immunotherapy: should they stick together? Br J Cancer. 2022;126: 1–3. doi:10.1038/s41416-021-01618-0

9. Arunachalam PS, Scott MKD, Hagan T, Li C, Feng Y, Wimmers F, et al. Systems vaccinology of the BNT162b2 mRNA vaccine in humans. Nature. 2021;596: 410–416. doi:10.1038/s41586-021-03791-x

10. Rinchai D, Deola S, Zoppoli G, Kabeer BSA, Taleb S, Pavlovski I, et al. High-temporal resolution profiling reveals distinct immune trajectories following the first and second doses of COVID-19 mRNA vaccines. Sci Adv. 2022;8:

eabp9961. doi:10.1126/sciadv.abp9961

11. Lee HK, Hoechstetter MA, Buchner M, Pham TT, Huh JW, Müller K, et al. Analysis of immune responses in patients with CLL after heterologous COVID-19 vaccination. Blood Adv. 2023;7: 2214–2227. doi:10.1182/bloodadvances.2022008445

12. Chaussabel D, Quinn C, Shen J, Patel P, Glaser C, Baldwin N, et al. A modular analysis framework for blood genomics studies: application to systemic lupus erythematosus. Immunity. 2008;29: 150–164. doi:10.1016/j.immuni.2008.05.012

13. Altman MC, Rinchai D, Baldwin N, Toufiq M, Whalen E, Garand M, et al. Development of a fixed module repertoire for the analysis and interpretation of blood transcriptome data. Nat Commun. 2021;12: 4385. doi:10.1038/s41467-021-24584-w

14. Rinchai D, Roelands J, Toufiq M, Hendrickx W, Altman MC, Bedognetti D, et al. BloodGen3Module: blood transcriptional module repertoire analysis and visualization using R. Bioinformatics. 2021;37: 2382–2389. doi:10.1093/bioinformatics/btab121

15. Martínez O, Reyes-Valdés MH. Defining diversity, specialization, and gene specificity in transcriptomes through information theory. Proc Natl Acad Sci U S A. 2008;105: 9709–9714. doi:10.1073/pnas.0803479105

16. Mulligan MJ, Lyke KE, Kitchin N, Absalon J, Gurtman A, Lockhart S, et al. Phase I/II study of COVID-19 RNA vaccine BNT162b1 in adults. Nature. 2020;586: 589–593. doi:10.1038/s41586-020-2639-4

17. Subramanian A, Tamayo P, Mootha VK, Mukherjee S, Ebert BL, Gillette MA, et al. Gene set enrichment analysis: a knowledge-based approach for interpreting genome-wide expression profiles. Proc Natl Acad Sci U S A. 2005;102: 15545–15550. doi:10.1073/pnas.0506580102

18. Liberzon A, Subramanian A, Pinchback R, Thorvaldsdóttir H, Tamayo P, Mesirov JP. Molecular signatures database (MSigDB) 3.0. Bioinformatics. 2011;27: 1739–1740. doi:10.1093/bioinformatics/btr260

19. Hadjadj J, Yatim N, Barnabei L, Corneau A, Boussier J, Smith N, et al. Impaired type I interferon activity and inflammatory responses in severe COVID-19 patients. Science. 2020;369: 718–724. doi:10.1126/science.abc6027

20. Le Bon A, Schiavoni G, D'Agostino G, Gresser I, Belardelli F, Tough DF. Type i interferons potently enhance humoral immunity and can promote isotype switching by stimulating dendritic cells in vivo. Immunity. 2001;14: 461–470. doi:10.1016/s1074-7613(01)00126-1

21. Gangaplara A, Martens C, Dahlstrom E, Metidji A, Gokhale AS, Glass DD, et al. Type I interferon signaling attenuates regulatory T cell function in viral infection and in the tumor microenvironment. PLoS Pathog. 2018;14: e1006985. doi:10.1371/journal.ppat.1006985

22. Chaussabel D, Baldwin N. Democratizing systems immunology with modular transcriptional repertoire analyses. Nat Rev Immunol. 2014;14: 271–280. doi:10.1038/nri3642

23. Huber JP, Farrar JD. Regulation of effector and memory T-cell functions by type I interferon. Immunology. 2011;132: 466–474. doi:10.1111/j.1365-2567.2011.03412.x

24. Nelli F, Signorelli C, Fabbri A, Giannarelli D, Virtuoso A, Giron Berrios JR, et al. Changes in Peripheral Immune Cells after the Third Dose of SARS-CoV-2 mRNA-BNT162b2 Vaccine and Disease Outcomes in Cancer Patients Receiving Immune Checkpoint Inhibitors: A Prospective Analysis of the Vax-on-Third-Profile Study. Cancers . 2023;15. doi:10.3390/cancers15143625

25. Graalmann T, Borst K, Manchanda H, Vaas L, Bruhn M, Graalmann L, et al. B cell depletion impairs vaccination-induced CD8+ T cell responses in a type I interferon-dependent manner. Ann Rheum Dis. 2021;80: 1537–1544. doi:10.1136/annrheumdis-2021-220435

26. Terao T, Naduka T, Ikeda D, Fukumoto A, Kamura Y, Kuzume A, et al. Depletion of CD38-positive regulatory T cells by anti-CD38 monoclonal antibodies induces a durable response to SARS-CoV-2 vaccination in patients with plasma cell dyscrasia. Br J Haematol. 2022;197: 417–421. doi:10.1111/bjh.18079

27. Kaplonek P, Wang C, Bartsch Y, Fischinger S, Gorman MJ, Bowman K, et al. Early cross-coronavirus reactive signatures of humoral immunity against COVID-19. Sci Immunol. 2021;6: eabj2901. doi:10.1126/sciimmunol.abj2901

28. Anderson EM, Goodwin EC, Verma A, Arevalo CP, Bolton MJ, Weirick ME, et al. Seasonal human coronavirus antibodies are boosted upon SARS-CoV-2 infection but not associated with protection. Cell. 2021;184: 1858–1864.e10. doi:10.1016/j.cell.2021.02.010

29. Grobben M, van der Straten K, Brouwer PJ, Brinkkemper M, Maisonnasse P, Dereuddre-Bosquet N, et al. Cross-reactive antibodies after SARS-CoV-2 infection and vaccination. Elife. 2021;10. doi:10.7554/eLife.70330

30. Rinchai D, Anguiano E, Nguyen P, Chaussabel D. Finger stick blood collection for gene expression profiling and storage of tempus blood RNA tubes. F1000Res. 2016;5: 1385. doi:10.12688/f1000research.8841.2

31. Yu G, Wang L-G, Han Y, He Q-Y. clusterProfiler: an R package for comparing biological themes among gene clusters. OMICS. 2012;16: 284–287. doi:10.1089/omi.2011.0118

32. Wu T, Hu E, Xu S, Chen M, Guo P, Dai Z, et al. clusterProfiler 4.0: A universal enrichment tool for interpreting omics data. Innovation (Camb). 2021;2: 100141. doi:10.1016/j.xinn.2021.100141

	C-FV (*N = 22*)	**RTX** (*N = 11*)	**ICI** (*N = 11*)
Age (IQR)	41 (*36 - 56*)	65 (*58 - 77*)	62 (*57 - 76*)
Sex			
Male	7 (*32%*)	6 (*55%*)	4 (*36%*)
Female	15 (*68%*)	5 (*45%*)	7 (*64%*)
Stage			
Early	-	7 (*64%*)	1 (9%)
Advanced	-	4 (*36%*)	9 (*82%*)
NA	-	-	1 (9%)
COVID-19			
COVID-19 diagnoses	9 (41%)	3 (*27%*)	1 (9%)
Pre-booster dose	2 (9%)	-	1 (9%)
Post-booster	7 (32%)	3 (27%)	-
Sampled participants			
Day 0	22	11	11
Day 1	22	11	11
Day 5	22	10	11
Week 4	22	9	11
Month 6	20	9	10
Median temporal interval Day 0 - Week 4 (IQR)	27 (*26 - 28*)	26 (*26 - 27*)	26 (*26 - 28*)
Median temporal	194 (*188.5 - 203*)	186 (175.5 - 194.5)	196 (*174 - 199.5*)

interval
Day 0 - Month 6
(IQR)

Table 1. Study cohort characteristics.

Figure legends

Figure 1. Humoral and cell-mediated immune responses after the third dose of the COVID-19 vaccine in C-FV, RTX, and ICI cohorts. A) Heatmap illustrating fold changes in Binding Antibody Index (BAI) for immunoglobulins targeting SARS-CoV-2 antigens: Envelope (Env), Nucleoprotein (Nucleo), Receptor Binding Domain (RBD), Full Spike Trimer (S-Trimer), and Spike S1 (S1). Red signifies an increase in BAI relative to baseline, while green denotes a decrease. Rows display immunoglobulin changes for IgM, total IgG, IgG subclasses (IgG1, IgG2, IgG3), and IgA subclasses (IgA1, IgA2), across time points (week 4 and month 6 versus baseline). The top annotation bar shows cumulative COVID-19 diagnosis status. B) Bar plots depicting unitary BAI changes at week 4 and month 6 versus baseline, with solid colors indicating adjustments for COVID-19 diagnosis in a mixed-effects model, and transparent colors for unadjusted estimates. C) Timeline highlighting the interval between vaccination and COVID-19 diagnosis in RTX patients, with month 6 total IgG-targeted BAI. D) Bar plots represent IGRA test results as percentages within each cohort, color-coded for positive (green), borderline (yellow), and negative (blue) outcomes at each time point.

Figure 2. Transcriptional profile following the booster dose of the COVID-19 vaccine in the C-FV cohort. (A) Fingerprint plot displaying the BloodGen3 module responses on days 1 and 5 relative to day 0, and on day 5 relative to day 1 in the C-

FC group. Modules are arranged in fixed positions, with each row (A1 to A38) representing a module aggregate. Red indicates modules with increased transcript levels compared to the reference time point; blue indicates decreased levels. The response percentage indicates the proportion of genes with increased or decreased abundance. Modules with a response between -15% and 15% are shown in white. (B) Bar plots summarizing the modular responses at each time point, with the upper plot showing the count of upregulated (red) and downregulated (blue) modules, and the lower plot showing the percentage of responsive modules. Each bar is color-coded by the functional category of the modules as indicated in the panel A legend. (C) Correlation matrix presenting Pearson correlation coefficients among BloodGen3 functional signatures, calculated using day 1 responses at the individual sample level.

Figure 3. Comparison of transcriptomic responses to the COVID-19 booster in C-FV and cancer patients. A),B) Bar plots displaying the number of upregulated (red) and downregulated (blue) modules at each time point contrast for RTX (A) and ICI (B) patients. The scatter plots show the percentage of module response on day 1 relative to day 0 for RTX and ICI patients (y-axis) against C-FV (x-axis). Each point, representing a Bloodgen3 module, follows the color scheme from Figure 2 for functional annotation, with points colored only if the response exceeds 15% or falls below -15%. C) Bar plots illustrating the relative module response for C-FV, RTX, and ICI patients on day 1 compared to day 0. D) Circos plot visualizing gene overlaps between upregulated TBD modules in RTX patients on day 1 and specific signatures, and highlighting the interconnectedness of responses across different patient groups.

Figure 4. Dissection of the interferon response in the different study cohorts. A) Dot plots showing the responses of A28/S1 (upper panel) and A28/S2 (lower panel) across study cohorts, with individual sample-level assessments. Each dot's color corresponds to the response percentage of A28/S1 or A28/S2, and lines indicate the average response for each module at each time point. B) Forest plot illustrating the interferon response on day 1 across cohorts, detailing the effects on A28/S1 and A28/S2 signatures and their modules.

Figure 5. Changes in blood cell composition in the different study cohorts on day 1 compared to day 0. Bar plots illustrating the variation in immune cell populations, analyzed using CIBERSORT, on day 1 relative to day 0 for each study cohort. Each bar indicates the fold change of specific cell populations from the baseline, covering a range of immune cells including B cells, T cells, NK cells, monocytes, dendritic cells, and others, across C-FV, RTX, and ICI cohorts.

Legends of Supplementary material

Supplementary Figures

Supplementary Figure 1. Sample collection and event timelines across C-FV, RTX, and ICI cohorts. This figure outlines the key milestones and sample collection points throughout the study period, spanning from 2020 through 2022. It includes timelines for vaccine administration (first dose, second dose, booster dose) and COVID-19 diagnosis events, alongside detailed sample collection moments (baseline, day 1, day 5, week 4, month 6). Each cohort's timeline is distinctly marked,

providing a clear visual representation of the study's temporal framework and the critical points for data collection and analysis.

Supplementary Figure 2. Humoral response to human coronaviruses (hCoVs) in different study cohorts. This figure presents a comprehensive analysis of the humoral immune response against various hCoV antigens, including HCoV-229E-S1, HCoV-HKU1-S1, HCoV-NL63-S1, HCoV-OC43-S1, MERS-S1, and SARS-S1, across C-FV, RTX, and ICI cohorts. The response is measured in terms of log2 fold change in Binding Antibody Index (BAI) at weeks 4 and 6 months post-vaccination, with separate panels for each hCoV antigen. It includes data for IgM, total IgG, IgG1, IgG2, IgG3, IgA1, and IgA2, visually depicted to highlight differences in immune response magnitude and specificity within and between patient cohorts.

Supplementary Figure 3. Correlations between SARS-CoV-2 and hCoV IgMs across study cohorts. Correlations between IgM responses to SARS-CoV-2 and various human coronaviruses (hCoVs), including HCoV-229E, HCoV-NL63, HCoV-OC43, and MERS-CoV. Through scatter plots, each panel depicts the correlation coefficients (rho) and significance levels (p-value) for IgM responses, highlighting the interconnectedness and potential cross-reactivity between responses to SARS-CoV-2 and other hCoVs.

Supplementary Figure 4. Fingerprint grid graph depicting the transcriptomic response to the COVID-19 booster in RTX and ICI patients. The figure is divided into panels comparing day 1 vs day 0, day 5 vs day 0, and day 5 vs day 1 for both RTX and ICI cohorts. Each panel represents a matrix with modules and response percentages, highlighting increases (red) and decreases (blue) in gene expression.

Supplementary Figure 5. Comparative analysis of transcriptomic responses in C-FV and cancer patients following the COVID-19 booster vaccine. A)

Comparison at day 5 versus day 0, showcasing the differential expression patterns and magnitude of response across the C-FV, RTX, and ICI cohorts. B) Day 5 versus day 1 comparisons, further delineating the temporal dynamics of gene expression changes induced by the booster shot.

Supplementary Figure 6. A) Correlation matrix of various immune deconvolution methods (e.g., CIBERSORT, MCP-counter) against whole blood count results, presenting their efficacy in mirroring actual blood cell counts. B) Changes in blood cell composition by CIBERSORT deconvolution on day 5 compared to day 0 across different study cohorts, using bar plots to display the fold change of various immune cell populations, thereby providing insights into how the COVID-19 booster affects immune cell dynamics within C-FV, RTX, and ICI patient groups.

Supplementary Tables

Supplementary Table 1. Extended data of study participants. Demographic and clinical information on the study participants across different cohorts (C-FV, RTX, and ICI). Data points include participant ID, group classification, age, sex, tumor type (where applicable), histology, stage of disease, type of therapy received, and steroid assumption. Additionally, it includes information on steroid administration type, presence of autoimmune diseases, comorbidities, vaccination status, and specific dates related to the study timeline (e.g., vaccination and sample collection dates). Serology and IGRA test results at various time points (Day 0, Day 5, Week 4, Month 6) are also documented, alongside intervals between the baseline and subsequent time points.

Supplementary Table 2. Humoral response to SARS-CoV-2 in different study cohorts. This table details the statistical analysis of the humoral immune response to SARS-CoV-2, as measured by the Binding Antibody Index (BAI) across various immunoglobulins (IgM, IgG, IgG1, IgG2, IgG3) and their specificities (e.g., SARS-CoV-2 Envelope). For each antibody, the table provides the time regression coefficient, indicating the change in BAI over time, and the COVID-19 regression coefficient, reflecting differences in BAI due to COVID-19 diagnosis. Statistical significance is assessed through p-values for both BAI over time (BAIt) and BAI relative to COVID-19 (BAI COVID-19), with adjustments for multiple testing presented as False Discovery Rate (FDR) values. The "Time point contrast" column specifies the comparison timeframe, such as "Week 4 | Baseline," facilitating an understanding of antibody dynamics post-vaccination.

Supplementary Table 3. Humoral Response to human coronaviruses (hCoVs) in different study Cohorts. This table outlines the detailed analysis of the humoral immune response against antigens from various hCoVs, such as SARS-CoV, measured through the Binding Antibody Index (BAI) for different immunoglobulin classes (IgM, IgG, IgG1, IgG2, IgG3). It provides an overview of the time regression coefficient for each antibody, reflecting changes in BAI over the study period, alongside the COVID-19 regression coefficient, indicating the impact of a COVID-19 diagnosis on antibody levels. The statistical significance of these changes is evaluated by p-values for BAI over time and in relation to COVID-19 diagnosis, with corrections for multiple comparisons through False Discovery Rate (FDR) values. Each entry is contextualized within a specific time point contrast, such as "Week 4| Baseline".

Supplementary Table 4. Results of IGRA assays. This table presents the outcomes of the Interferon-γ Release Assay (IGRA) for measuring immune responses in study participants across different cohorts (C-FV, RTX, ICI). It includes subject IDs, group categorization, and quantitative IGRA results (expressed in mIU/mL) at various time points: Day 0 (pre-booster), Day 5, Week 4, and Month 6 post-booster vaccination. Values exceeding the assay's upper limit of quantification are indicated by ">1900 mIU/mL".

Supplementary Table 5. Immune module response at each time point contrast in the different study cohorts. Responses of the immune modules, evaluated through transcriptomic analysis, across various time points (Day 1 vs. Day 0, Day 5 vs. Day 0, Week 4 vs. Day 0, Month 6 vs. Day 0) in the study cohorts (C-FV, RTX, ICI). For each immune module, the table outlines the fold changes, statistical significance, and direction of response (upregulation or downregulation) at each contrasted time point.

Acknowledgments: AIRC, AIL, 5x1000 (HSM), RC IRCCS (HSM), ACC, Fondi di Ricerca Ateneo (UniGE), donazioni liberali (Grazia Benvenuto e Piero Chiabra), PRIN, intellectual insights by Dr. P. Blandini, MD

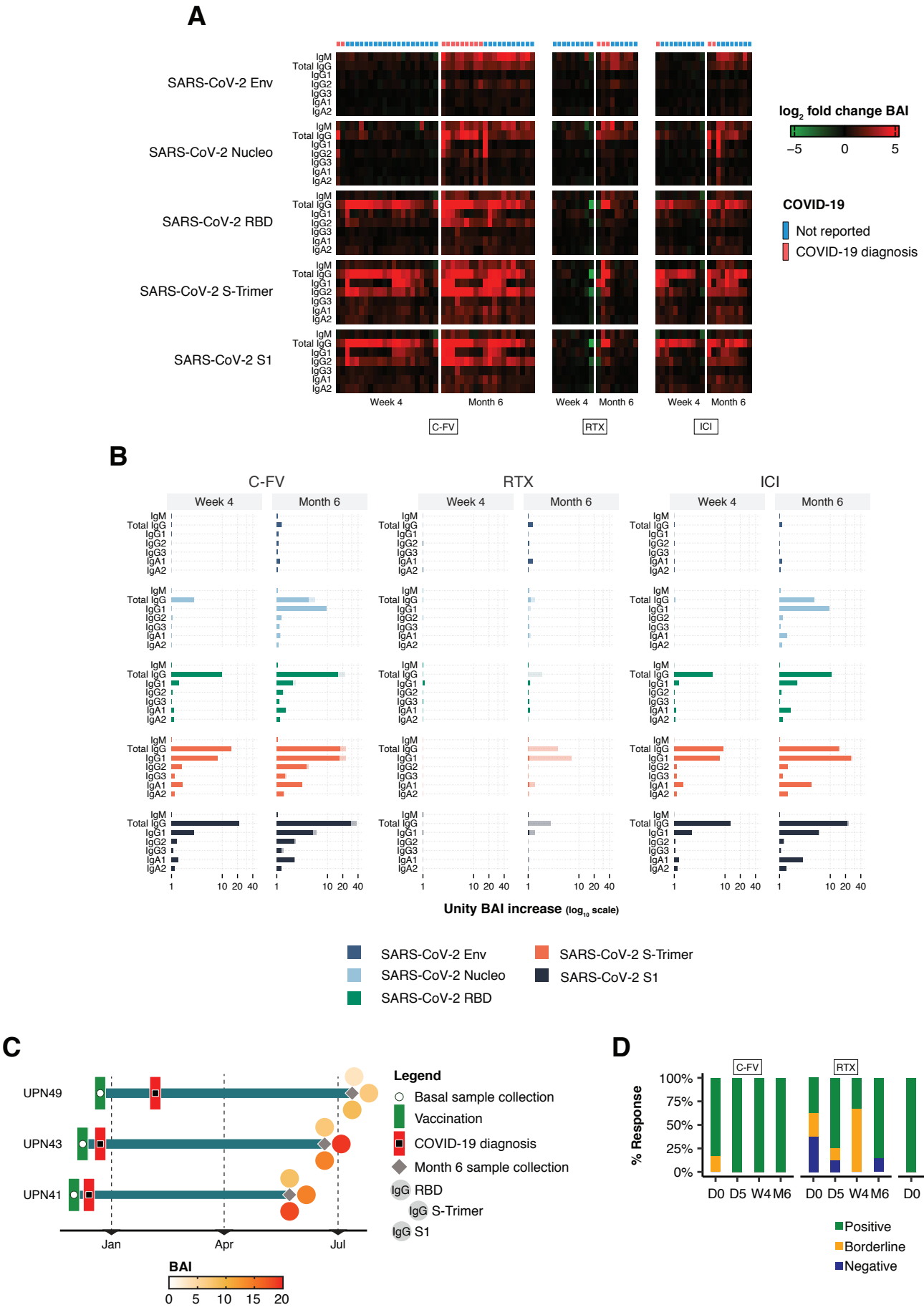
A
SARS-CoV-2 Env
SARS-CoV-2 Nucleo
SARS-CoV-2 RBD
SARS-CoV-2 S-Trimer
SARS-CoV-2 S1
IgM
Total IgG
IgG1
IgG2
IgG3
IgA1
IgA2
Week 4
Month 6
C-FV
RTX
ICI
log2 fold change BAI
−5
0
5
COVID-19
Not reported
COVID-19 diagnosis
B
C-FV
RTX
ICI
Week 4
Month 6
1
10
20
40
Unity BAI increase (log10 scale)
SARS-CoV-2 Env
SARS-CoV-2 Nucleo
SARS-CoV-2 RBD
SARS-CoV-2 S-Trimer
SARS-CoV-2 S1
C
UPN49
UPN43
UPN41
Jan
Apr
Jul
BAI
0
5
10
15
20
Legend
Basal sample collection
Vaccination
COVID-19 diagnosis
Month 6 sample collection
IgG RBD
IgG S-Trimer
IgG S1
D
C-FV
RTX
ICI
% Response
100%
75%
50%
25%
0%
D0
D5
W4
M6
Positive
Borderline
Negative

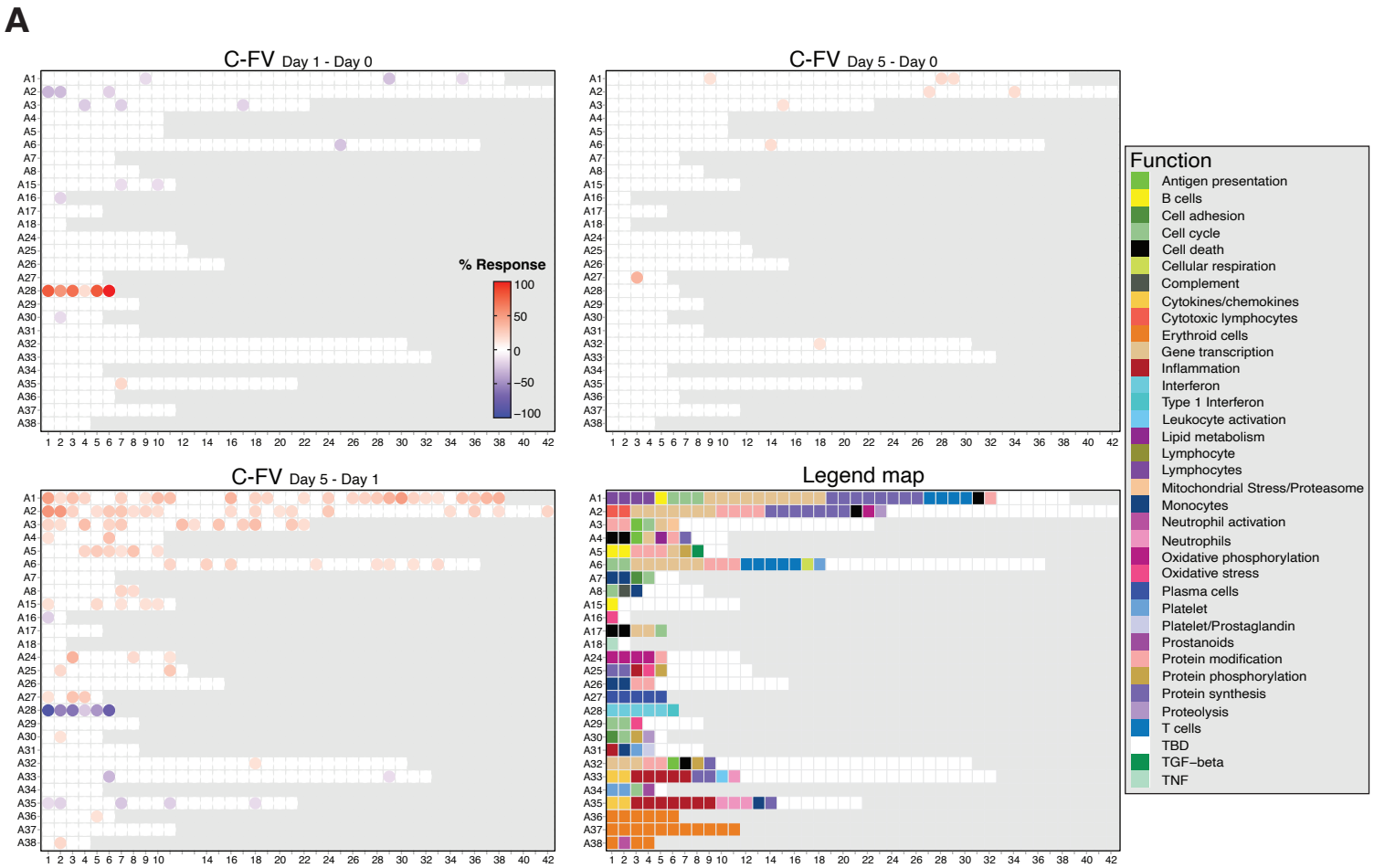
A
C-FV Day 1 - Day 0
C-FV Day 5 - Day 0
C-FV Day 5 - Day 1
Legend map
% Response
100
50
0
−50
−100
Function
Antigen presentation
B cells
Cell adhesion
Cell cycle
Cell death
Cellular respiration
Complement
Cytokines/chemokines
Cytotoxic lymphocytes
Erythroid cells
Gene transcription
Inflammation
Interferon
Type 1 Interferon
Leukocyte activation
Lipid metabolism
Lymphocyte
Lymphocytes
Mitochondrial Stress/Proteasome
Monocytes
Neutrophil activation
Neutrophils
Oxidative phosphorylation
Oxidative stress
Plasma cells
Platelet
Platelet/Prostaglandin
Prostanoids
Protein modification
Protein phosphorylation
Protein synthesis
Proteolysis
T cells
TBD
TGF−beta
TNF

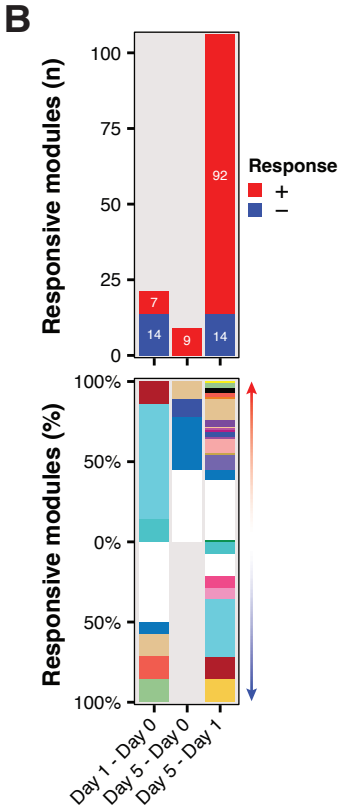
B
Responsive modules (n)
Responsive modules (%)
Response
+
−
92
7
14
9
14
Day 1 - Day 0
Day 5 - Day 0
Day 5 - Day 1

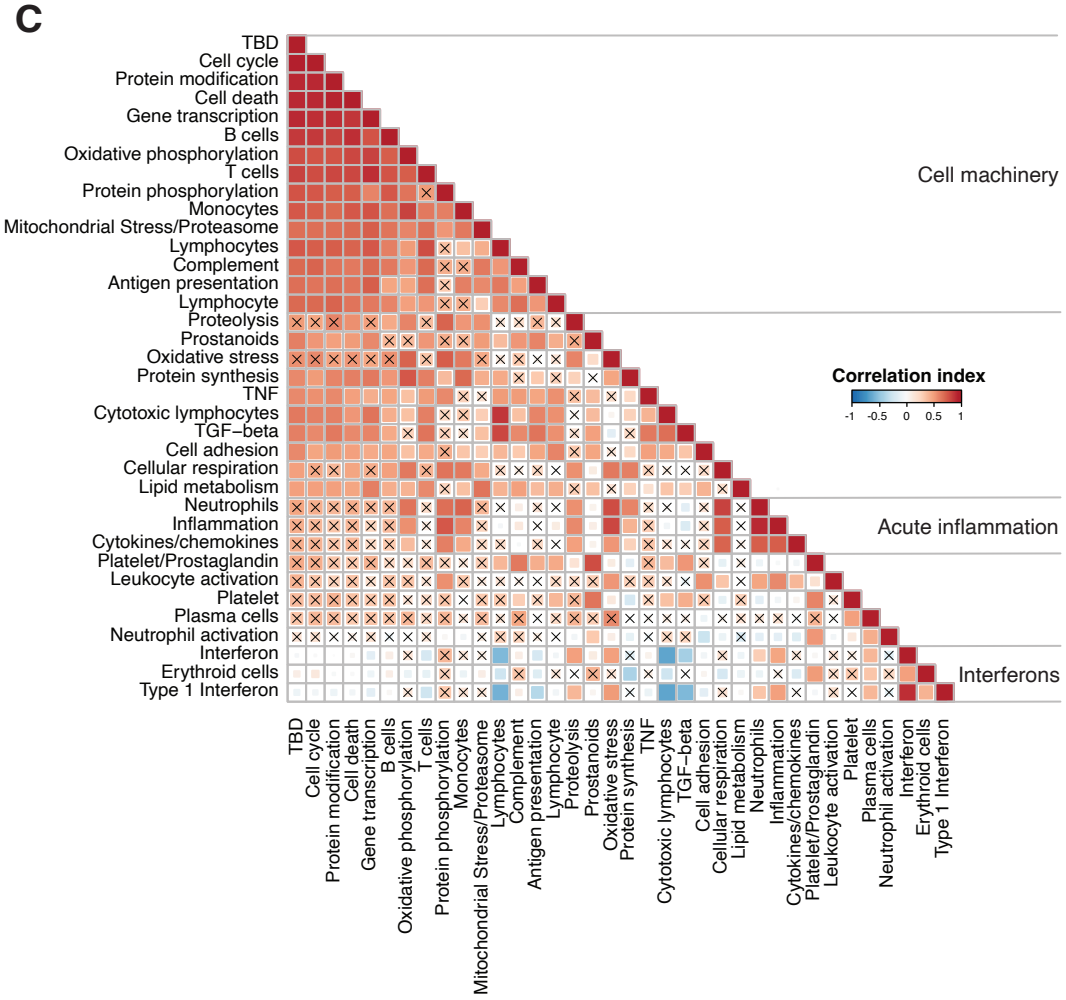
C
Cell machinery
Acute inflammation
Interferons
Correlation index
-1
-0.5
0
0.5
1
TBD
Cell cycle
Protein modification
Cell death
Gene transcription
B cells
Oxidative phosphorylation
T cells
Protein phosphorylation
Monocytes
Mitochondrial Stress/Proteasome
Lymphocytes
Complement
Antigen presentation
Lymphocyte
Proteolysis
Prostanoids
Oxidative stress
Protein synthesis
TNF
Cytotoxic lymphocytes
TGF−beta
Cell adhesion
Cellular respiration
Lipid metabolism
Neutrophils
Inflammation
Cytokines/chemokines
Platelet/Prostaglandin
Leukocyte activation
Platelet
Plasma cells
Neutrophil activation
Interferon
Erythroid cells
Type 1 Interferon

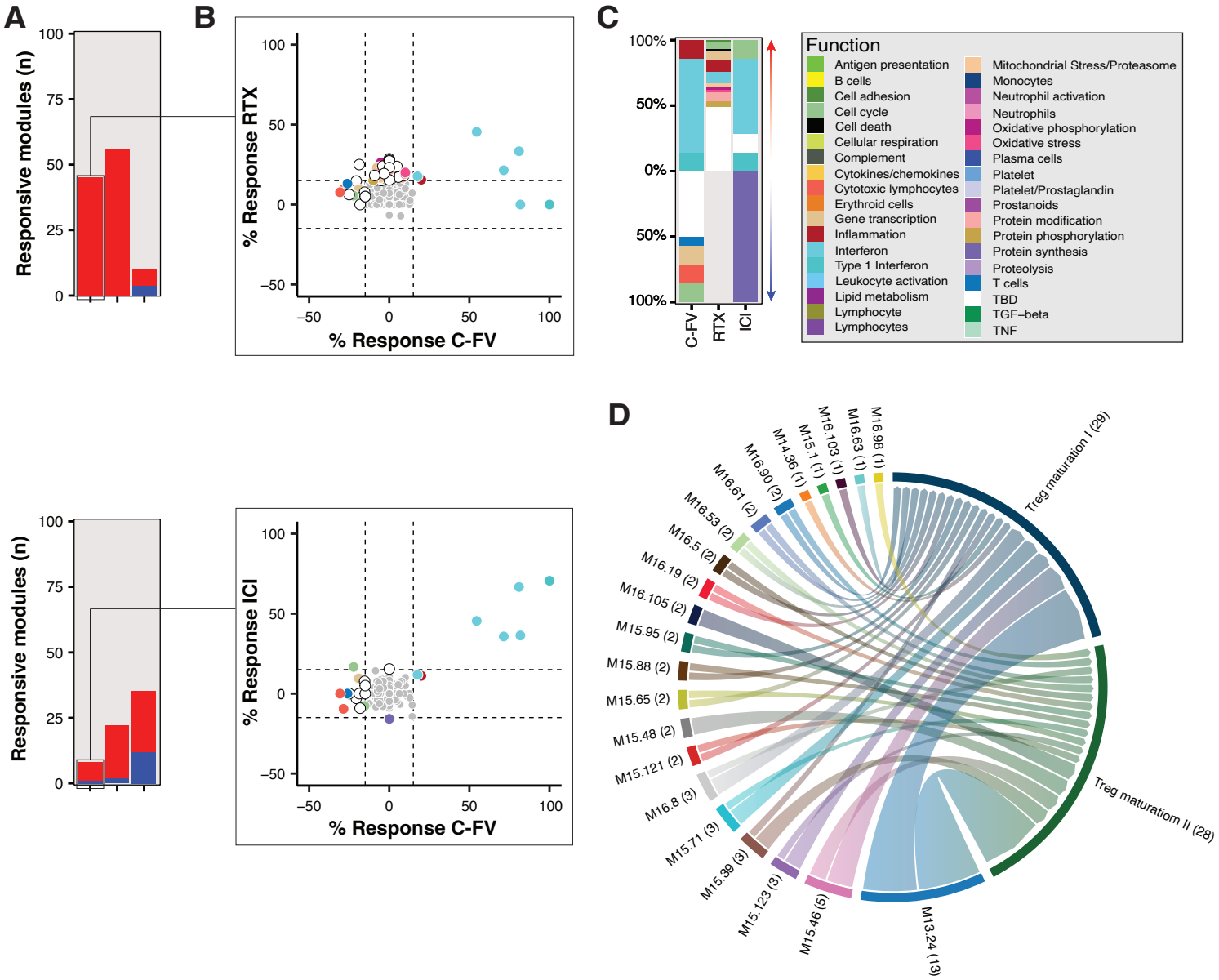
A
B
C
D
Responsive modules (n)
% Response RTX
% Response C-FV
% Response ICI
C-FV
RTX
ICI
Function
Antigen presentation
B cells
Cell adhesion
Cell cycle
Cell death
Cellular respiration
Complement
Cytokines/chemokines
Cytotoxic lymphocytes
Erythroid cells
Gene transcription
Inflammation
Interferon
Type 1 Interferon
Leukocyte activation
Lipid metabolism
Lymphocyte
Lymphocytes
Mitochondrial Stress/Proteasome
Monocytes
Neutrophil activation
Neutrophils
Oxidative phosphorylation
Oxidative stress
Plasma cells
Platelet
Platelet/Prostaglandin
Prostanoids
Protein modification
Protein phosphorylation
Protein synthesis
Proteolysis
T cells
TBD
TGF–beta
TNF
Treg maturation I (29)
Treg maturation II (28)
M16.98 (1)
M16.63 (1)
M16.103 (1)
M15.1 (1)
M14.36 (1)
M16.90 (2)
M16.61 (2)
M16.53 (2)
M16.5 (2)
M16.19 (2)
M16.105 (2)
M15.95 (2)
M15.88 (2)
M15.65 (2)
M15.48 (2)
M15.121 (2)
M16.8 (3)
M15.71 (3)
M15.39 (3)
M15.123 (3)
M15.46 (5)
M13.24 (13)

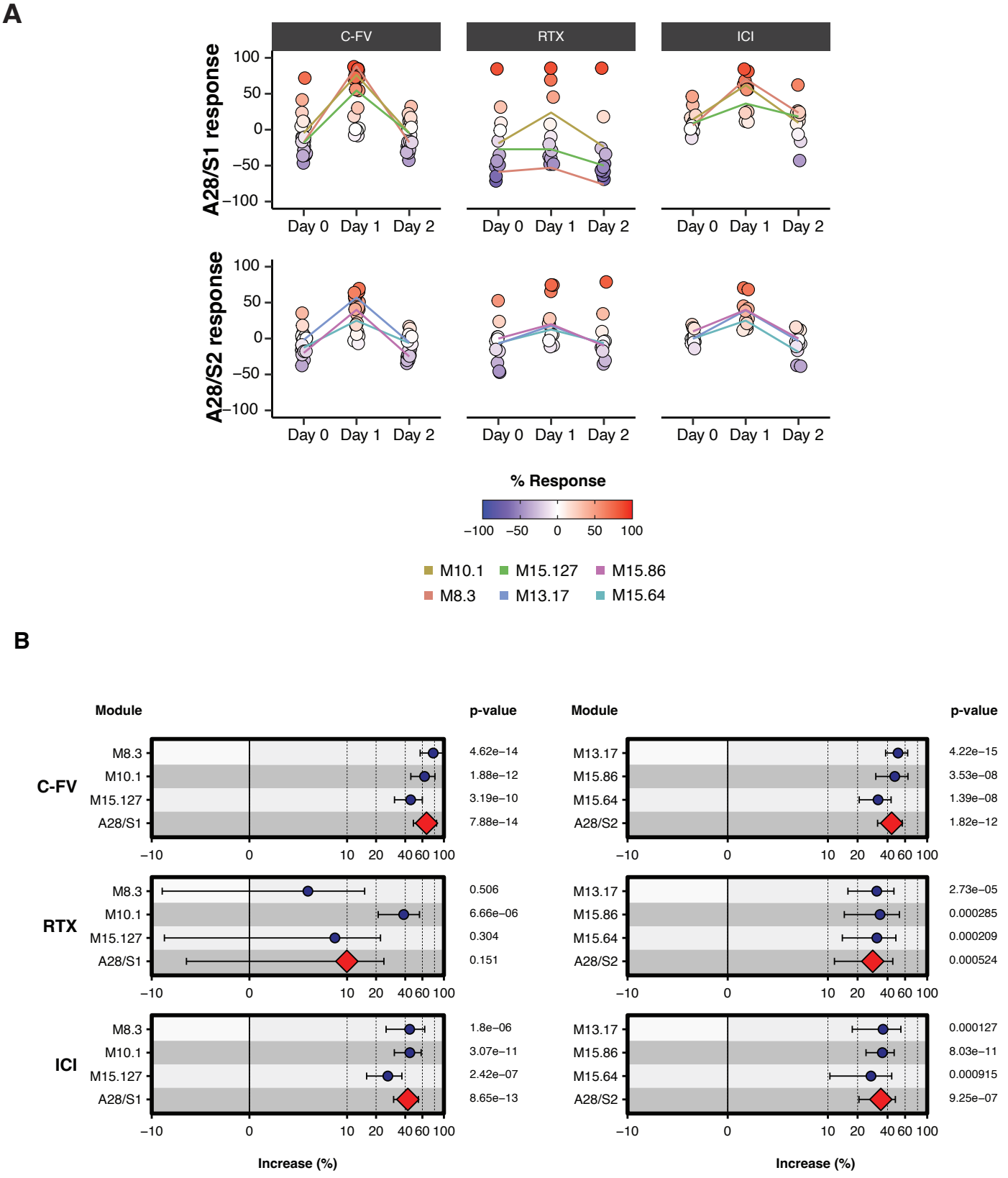
A
C-FV
RTX
ICI
A28/S1 response
A28/S2 response
100
50
0
−50
−100
Day 0
Day 1
Day 2
% Response
−100 −50 0 50 100
M10.1
M15.127
M15.86
M8.3
M13.17
M15.64
B
Module
p-value
C-FV
M8.3
M10.1
M15.127
A28/S1
4.62e−14
1.88e−12
3.19e−10
7.88e−14
RTX
0.506
6.66e−06
0.304
0.151
ICI
1.8e−06
3.07e−11
2.42e−07
8.65e−13
M13.17
M15.86
M15.64
A28/S2
4.22e−15
3.53e−08
1.39e−08
1.82e−12
2.73e−05
0.000285
0.000209
0.000524
0.000127
8.03e−11
0.000915
9.25e−07
−10 0 10 20 40 60 100
Increase (%)

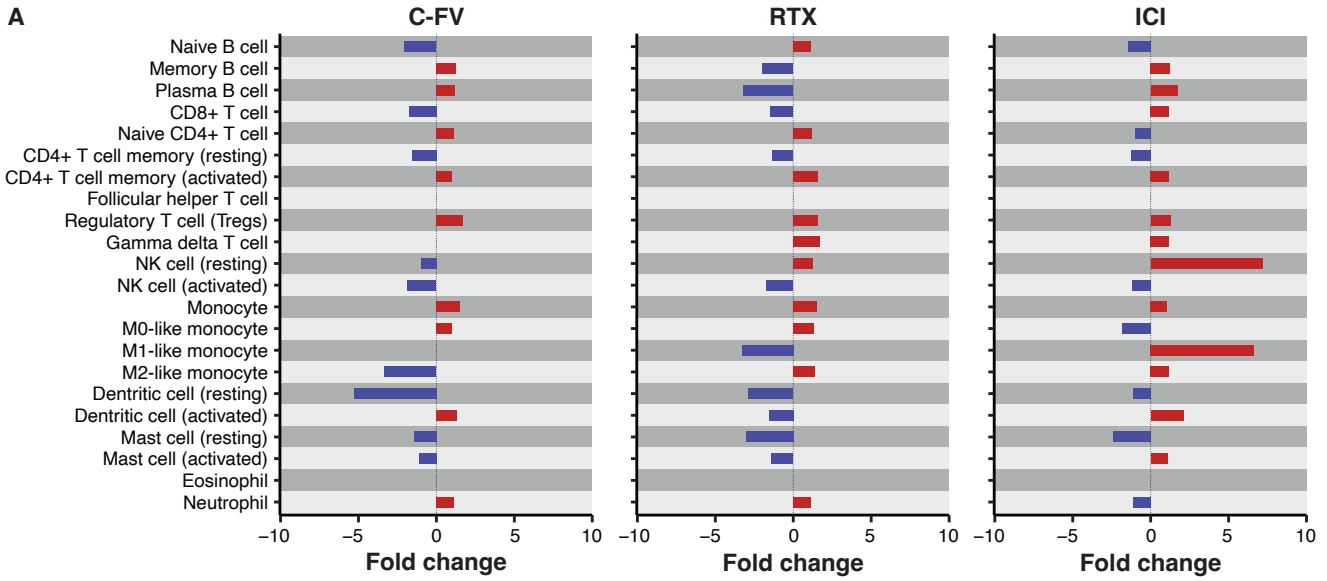
A
C-FV
RTX
ICI
Naive B cell
Memory B cell
Plasma B cell
CD8+ T cell
Naive CD4+ T cell
CD4+ T cell memory (resting)
CD4+ T cell memory (activated)
Follicular helper T cell
Regulatory T cell (Tregs)
Gamma delta T cell
NK cell (resting)
NK cell (activated)
Monocyte
M0-like monocyte
M1-like monocyte
M2-like monocyte
Dentritic cell (resting)
Dentritic cell (activated)
Mast cell (resting)
Mast cell (activated)
Eosinophil
Neutrophil
−10
−5
0
5
10
Fold change